Lattice Boltzmann Method Simulations of Stokes Number Effects on Particle Trajectories in a Wall-Bounded Flow

Anand Samuel Jebakumar[a,*], Kannan N. Premnath[b], John Abraham[a,c]

[a] *School of Mechanical Engineering, Purdue University, West Lafayette, IN, 47906, USA*
[b] *Department of Mechanical Engineering, University of Colorado, Denver, CO 80217, USA*
[c] *School of Mechanical Engineering, University of Adelaide, Adelaide, South Australia 5005, Australia*

Abstract

Experimental studies of particle-laden flows in a pipe show that the spatial distribution of the particles across the radius of the pipe is dependent on the Stokes number [Timothy C. W. Lau & Graham J. Nathan, J. Fluid Mech. 2014]. It has been suggested that the Saffman lift effect [Saffman, P. G., J. Fluid Mech. 1965] makes a significant contribution to this spatial distribution. The Saffman lift effect has been studied in prior works by several authors and the relative contribution of the lift force has been studied within the context of various forces acting on particles in a flow. The lift force depends on the particle size and the velocity of the particle relative to the gas phase. In this study, the lattice Boltzmann method is employed to study the mechanism of particle migration of an isolated particle moving in a wall-bounded flow. The boundary condition proposed by Bouzidi *et al.* [Phys. Fluids, 2001], which involves the bounce-back scheme modified to account for fractional link distances between the wall and the fluid node, is used for the particles. The force acting on the particle is found by adding the momentum lost by all the fluid molecules as they bounce back from the particle surface along the link joining the particle and the fluid boundary nodes. This force is used to update the position of the particle after

*Corresponding author
Email address: ajebakum@purdue.edu (Anand Samuel Jebakumar)

every streaming step. The torque acting on the particle is determined similarly and is used to update the angular velocity of the particle. It is found that at low Stokes number the particle behaves like a neutrally buoyant particle and exhibits the Segré-Silberberg effect. With increasing Stokes number, the particle exhibits an oscillatory behavior about its mean position. For large Stokes number, the particle oscillations are significant. If the ratio of channel height to particle diameter is increased, the particle moves closer to the wall and the oscillatory behavior is evident at lower Stokes number.
Keywords: Lattice Boltzmann method, particle-laden flow, Saffman lift, Stokes number effects

1. Introduction

Particle-laden flows are common in several industrial devices such as coal combustors, gasifiers, fluidized bed reactors, and pharmaceutical delivery systems. In these devices, particles are invariably transported by a carrier fluid. For example, when particles are delivered to a gasifier, these particles are carried by a stream of air through a pipe. It is, of course, desirable to avoid deposition of particles on the walls of the pipe as this can affect the particle flow rates and distribution. The uniformity of the particle distribution in the pipe and at the exit of the pipe is an important consideration in the design of the delivery system and possibly in the performance of the gasifier. Computational Fluid Dynamic (CFD) models are extensively employed to understand the performance of these devices and optimize them. In these CFD models, prescribing the boundary and initial conditions are critical. Exit velocity profiles and particle distribution profiles are often prescribed as boundary conditions.

Particle migration in pipes has been studied by several researchers in the past. Segré and Silberberg [1, 2] observed that a neutrally buoyant particle in a pipe flow migrates to a position that is between the axis and the pipe wall. Bretherton [3] has showed through an analytical study that this migration does not occur if the inertial term in the Navier-Stokes equation is neglected. The

analysis of Bretherton was for a rigid spherical particle at low Reynolds (Re) number, i.e. in the Stokes flow limit. Saffman [4] investigated the effects of inertia using perturbation analysis and found that a particle in a linear unbounded shear flow experiences a lateral force. Hence, lateral migration arises due to an inertial force at non-zero Re number. This force is generally referred to as Saffman lift and denotes the force acting on a particle on account of a velocity gradient across it in a direction perpendicular to the flow when the particle leads or lags the flow. The Saffman lift force tends to push a particle that leads the fluid into a region with lower velocity and vice versa. McLaughlin [5] analyzed the inertial lift acting on a particle in a wall-bounded linear shear flow.

Feng *et al.* [6, 7] have performed two-dimensional numerical simulations of circular particles settling in a channel with no mean flow, transported in a Couette flow and in a Poiseuille flow. For a particle in a channel flow, they were able to observe the Segré-Silberberg effect. They identified Saffman lift (corrected to account for the velocity profile curvature of an undisturbed Poiseuille flow), Magnus lift, and wall repulsion to be the dominant forces that cause the particle migration. They have reported the dependence of the particle migration trajectories on parameters such as the Re number (based on the particle diameter), the ratio of channel height to the particle diameter (H/d ratio) and the density ratio of the particle to the fluid. Mortazavi and Tryggvason [8] performed similar simulations with deformable drops in a channel flow. They observed that at high Re numbers, the drops began to oscillate about the center of the channel. Zeng *et al.* [9] performed numerical simulations of a spherical particle in a wall-bounded flow and studied the dependence of the lift-coefficient on the particle Re number. Nourbakhsh *et al.* [10] have done 3D simulations of drops in a Poiseuille flow and have studied the effect of capillary number, Re number and the volume fraction on the drop migration. However, to the best knowledge of the authors, the effect of Stokes number on the particle migration trajectories has not been reported in the literature.

The Stokes (St) number is the ratio of particle response time to the flow response time. A particle with a low St number adjusts itself to the flow almost

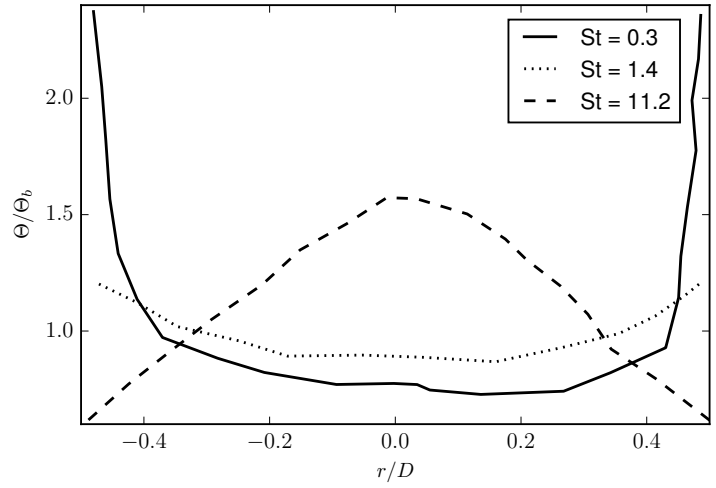

Figure 1: Radial concentration of particles for various St numbers in a turbulent pipe flow [11]

instantaneously whereas a particle with a high St number takes a long time to accommodate to the flow. In a recent study by Lau and Nathan [11], it was observed that particles in a pipe flow tend to migrate preferentially either toward or away from the wall depending on their St number. Figure 1 shows the concentration of particles Θ, normalized by the bulk concentration Θ_b, as a function of the radial distance at the exit of a turbulent pipe flow from the work of Lau and Nathan [11]. It can be seen that particles with low St number are concentrated near the walls while particles with high St number are concentrated near the axis. The response time τ_p for a spherical particle at low Reynolds number is given by [12] as

$$\tau_p = \frac{(2\rho_p + \rho_f)d_p^2}{36\mu}, \tag{1}$$

where ρ_p is the density of the particle, ρ_f is the density of the fluid, d_p is the diameter of the particle and μ is the viscosity of the fluid. If the particle density is much higher than the fluid density, this reduces to

$$\tau_p = \frac{\rho_p d_p^2}{18\mu}. \tag{2}$$

This can be expressed alternatively as

$$\tau_p = \frac{d_p^2}{18\nu}\left(\frac{\rho_p}{\rho_f}\right), \tag{3}$$

where ν is the kinematic viscosity of the fluid. This expression brings in a ratio of the particle density to the fluid density. The flow response time can be obtained from a characteristic length scale L_c and velocity scale U_c of the bulk flow as

$$\tau_f = \frac{L_c}{U_c}. \tag{4}$$

For a pipe flow, the characteristic velocity U_c can be taken as the maximum velocity U_{max} and the diameter of the pipe D can be taken as the characteristic length scale L_c. This gives an expression for St number as

$$St = \frac{\rho_p d_p^2 U_{max}}{18\mu D}. \tag{5}$$

For a channel flow, the channel height H can be taken as a characteristic length scale, yielding an expression for St number as

$$St = \frac{\rho_p d_p^2 U_{max}}{18\mu H}. \tag{6}$$

The aim of this work is to understand the effect of St number on the migration trajectories of particles in a channel flow by carrying out Direct Numerical Simulations (DNS) with the particle itself being numerically resolved.

In this study, we employ the lattice-Boltzmann method (LBM) to study the motion of particles in a channel flow. Ladd [13, 14] was the first to carry out a particle-laden flow simulation using the LBM. Ladd performed simulations in the creeping flow regime as well as for low Reynolds number (Re) flows. Aidun *et al.* [15] have done simulations on particles, whose density is close to that of the fluid. Qi *et al.* [16, 17, 18, 19] have also carried out LBM simulations of various flows with circular, elliptical and rectangular particles as well as three-dimensional cylindrical particles.

In the studies listed above [13, 14, 15, 16, 17, 18, 19], a staircase approximation is used to represent the particle when its boundary is curved. This

approximation does not preserve the boundary representation of the particle as it moves in the fluid. Feng and Michaelides [20, 21, 22] used Immersed Boundary Method (IBM) in order to overcome this issue. Bouzidi *et al.* [23] proposed an alternate method that accounts for the fractional link distances as the particle cuts across different lattice links. This method is simple to implement and preserves the particle boundary representation as it moves across the lattices. This ensures that the particle does not experience any force fluctuations. Other LBM works on particulate flows are listed in Refs. [24, 25, 26, 27]. Reference [28] may be consulted for a comprehensive review of LBM studies of particle-laden flows.

The main goal of this work is to study the migration trajectories of particles in a channel flow and to examine the influence of St number on the trajectories. We will examine the fundamental mechanisms responsible for this migration. The rest of the paper is organized as follows: The computational method employed is discussed in the next section. We will then assess the accuracy of the method through comparisons with prior works. The results from our study are then presented and the mechanism of particle migration is explained. The paper closes with summary and conclusions.

2. Computational Method

As indicated earlier, the LBM is employed for our computations with a two-dimensional D2Q9 lattice for the discrete velocities. Figure 2 shows a D2Q9 lattice. References [15, 23, 29, 30, 31] may be consulted for information on the specific implementation of particle motion as well as the boundary conditions. A brief description is given here.

The LBM is a kinetic solver that solves for the velocity distribution function. It is derived from the Boltzmann Equation by discretizing the velocity space with finite velocities. The Boltzmann equation is

$$\frac{Df}{Dt} = \frac{\partial f}{\partial t} + \vec{c} \cdot \nabla_{\vec{x}} f + \vec{F} \cdot \nabla_{\vec{c}} f = C_{12} \tag{7}$$

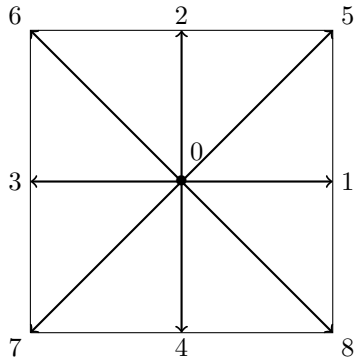

Figure 2: Schematic of a D2Q9 lattice

where f is the single particle velocity distribution function, t is time, $\vec{c}$ is the particle speed, $\nabla_{\vec{x}}$ and $\nabla_{\vec{c}}$ represent the gradient with position and velocity space and $\vec{F}$ represents external forces. In our computations, there is no external force. C_{12} represents the effect of two particle collisions. For our computations, the BGK collision operator is used to represent the effect of intermolecular collisions. The discrete form of the Boltzmann equation is

$$f_i(\vec{x} + \vec{c_i}\delta_t, t + \delta_t) - f_i(\vec{x}, t) = -\frac{1}{\tau}[f_i(\vec{x}, t) - f_i^{eq}(\vec{x}, t)] \tag{8}$$

where f_i represents the distribution function in the discrete direction i, $\vec{c_i}$ is the corresponding velocity, τ is the relaxation parameter and f_i^{eq} is the discretized version of the Maxwellian equilibrium distribution function. The right hand side of Eq. 8 represents the BGK collision operator. In the LBM, the fluid molecules are constrained to move only in certain directions. Chen *et al.* [32] have shown by performing a Taylor-series expansion in time and space and by using the Chapman-Enskog expansion that the Navier-Stokes equations can be recovered from the LB equations.

The boundary representation of the particle in the lattice is implemented as follows: In the LBM, a no-slip boundary condition can be achieved by placing a wall halfway between the last fluid node and an imaginary boundary node and allowing the fluid molecules to bounce on the wall and return to its initial node

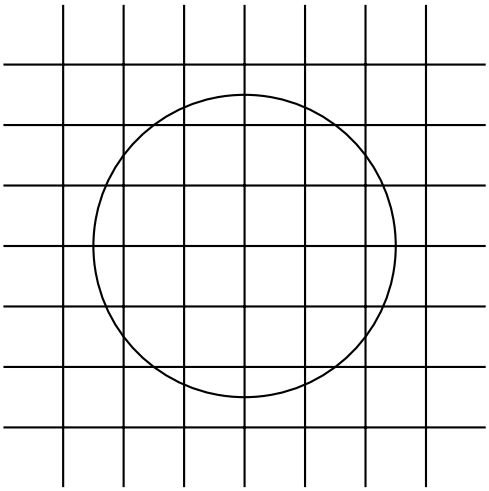

Figure 3: A particle in a D2Q9 lattice

with a velocity in the opposite direction. He *et al.* [33] have shown that a bounce back scheme with the wall placed halfway between the last fluid node and an imaginary boundary node gives second-order accurate results. However, owing to the curved surface of the particle, it cuts the lattices at different distances and not halfway as shown in Fig. 3 Hence, the halfway bounce-back scheme cannot be used as originally proposed. Bouzidi *et al.* [23] proposed a scheme that accounts for the fractional link distances. This scheme is used in our computations.

In order to find the force acting on the particle due to fluid drag, the momentum exchange technique, similar to that employed by Mei *et al.* [29], is used. In this method, the momentum transferred by the fluid molecules to the solid particle as it bounces back from the surface of the particle is summed up to get the total momentum transferred to the particle in a time step. As the particle moves in the computational domain, some of the fluid nodes would be uncovered while some may be covered. In such cases, the density of the newly appeared fluid node is obtained as the average density of all the neighboring fluid nodes. The velocity of the uncovered node is equal to the sum of the velocity of the

particle and the angular velocity times the position vector joining the lattice node and the particle center. From this velocity and density, the equilibrium distribution functions are calculated and are assigned as the distribution functions of this node. This newly created fluid node gains some momentum. The particle momentum should therefore decrease by the same amount to ensure momentum conservation. Similarly, when a particle covers a fluid node, it gains the momentum of the fluid node at that instant. These forces due to a particle covering and uncovering a fluid node are added to the force found by the momentum exchange method and is used to update the velocity and position of the particle. This technique gives rise to fluctuations in the force acting on the particle as it moves across the lattice nodes. Figure 4 shows the instantaneous and averaged force acting on the particle in both the direction parallel to the wall and normal to it during one of the computations. It is seen that there is a high frequency fluctuation (black line) that arises due to the particle covering and uncovering fluid nodes. The red line shows the time average of this force over a time span t_s, where t_s represents the time taken by the fluid to traverse a distance equal to the radius of the particle (r_p/U). The particle motion however, depends on the averaged force and is not influenced significantly by these high frequency fluctuations. The torque acting on the particle is found out similarly and is used to update the angular velocity of the particle. It should be noted that the particle rotation would not change its orientation but would change the fluid velocity at its boundary. Ref. [15] may be consulted for a detailed explanation of the particle motion implementation

The computational domain used in our simulations is shown in Fig. 5. The length of the domain is 70H, where H is the height of the channel. The particle is released at 10H axial distance from the inlet and data is taken only until an axial distance of 60H. These dimensions are selected based on the results of Feng *et al.* [6]. We have carried out multiple simulations to ensure that the particle migration trajectories are not influenced by the inlet and outlet boundary conditions. At the inlet, a parabolic velocity profile corresponding to an undisturbed Poiseuille flow is specified. At the outlet, stress-free boundary

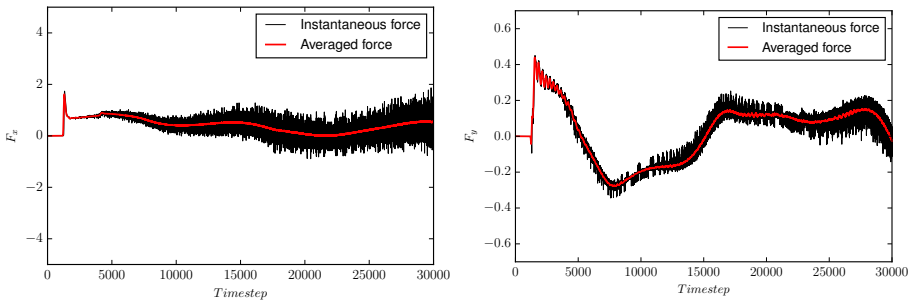

(a) (b)

Figure 4: Hydrodynamic forces acting on the particle: a) Force in the direction parallel to the wall b) Force in the direction normal to the wall.

conditions are specified. These are implemented by means of the extrapolation method proposed by Chen *et al.* [30].

The particle is resolved by having 25 lattice points across its diameter for the channel flow case. Increasing the number of grid points across the particle is found to have no noticeable effect on the particle migration trajectories. In all of our computations, there exists at least 3 lattice points between the particle and the wall. This ensures that the lubrication forces are completely resolved thereby eliminating the need for including explicit lubrication corrections.

3. Assessment of the Computational Method

In order to assess the computational method outlined above, we compare our simulation results with those of Feng *et al.* [6, 7] for the case of a particle settling in a channel under the action of an imposed force (gravity), i.e. sedimentation, and a particle in a channel flow. The simulations of Feng *et al.* are two-dimensional with the fluid motion computed by solving the Navier-Stokes equation with a finite element solver.

3.1. Sedimentation

In this simulation, a particle is allowed to sediment between two walls under the action of an imposed force. The force acts in a direction parallel to the wall.

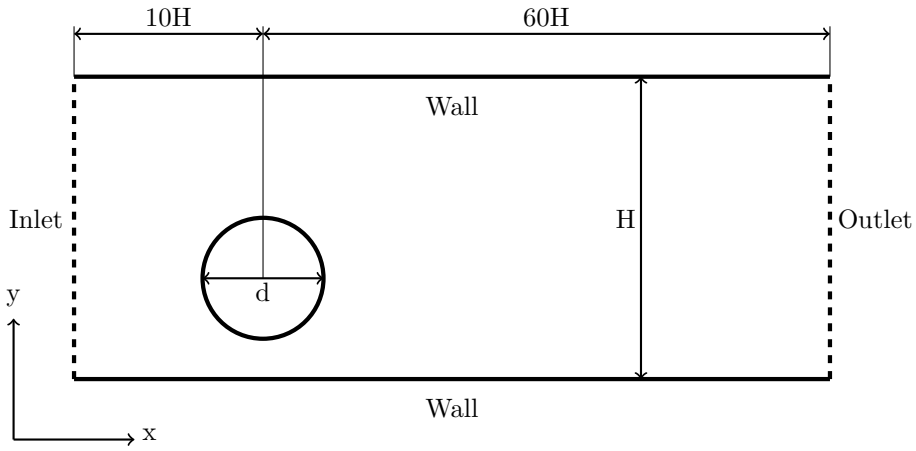

Figure 5: Computational domain

As the particle settles, it will accelerate until it acquires a terminal velocity. A Reynolds (Re) number is defined based on the particle diameter d_p and its terminal velocity v_p as

$$Re = \frac{\rho v_p d_p}{\mu} \tag{9}$$

where ρ is the density of the fluid and μ is the viscosity of the fluid. A schematic of this setup is shown in Fig. 6. The particle is released from different 'y' locations during different simulations.

Based on the value of the Re number, Feng *et al.* [6] observed five distinct regimes of particle migration trajectories as listed in Table 1. At low Re number, the centerline of the channel would be the equilibrium position for the particle. When the Re number increases, the top down symmetry of the flow around the particle begins to vanish due to periodic vortex shedding. This causes the particle to oscillate. A detailed explanation of this particle migration is given in Ref. [6].

The first set of simulations we carried out with the LBM was to assess the method for the sedimentation problem. The particle is allowed to settle under the influence of a force which acts in a direction parallel to the walls. The H/d

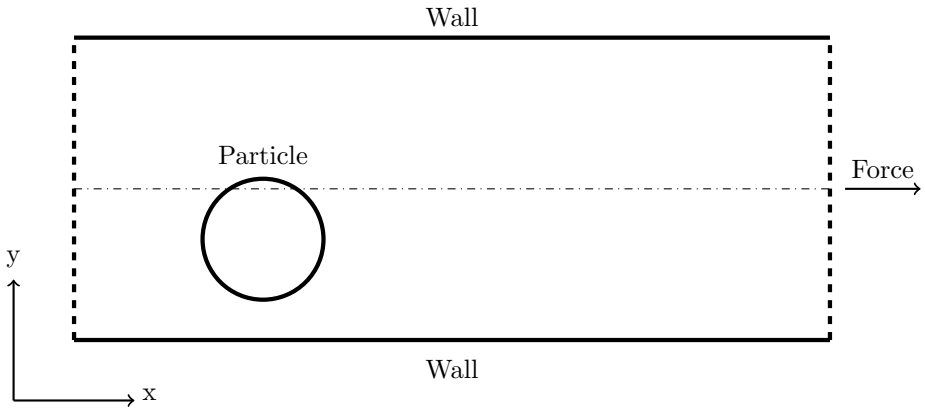

Figure 6: Schematic of setup for study of sedimentation of a particle

(channel width to particle diameter) ratio is the same as that used by Feng *et al.* [6]. The inlet and the outlet are specified as periodic boundary conditions. A qualitative comparison of results obtained from the LBM with that of Feng *et al.* [6] is presented in Fig. 7. The Re number is based on the particle terminal velocity as mentioned earlier. Hence, the Re number is not known a priori. This makes it difficult to perform a simulation where the Re number matches with that of Feng *et al.* [6]. In our computations, we have performed simulations where the Re number lies in a range where the particle behavior is similar to that observed by Feng *et al.* [6] and compared with their results. Hence, only a qualitative comparison can be made between the two figures. For this reason, the results are not plotted on the same graph.

It can be seen that for the regimes shown above, the LBM trends are in good agreement with that of Feng *et al.* Consider Figs. 7a and 7b. These figures show results for low Re when the particle migrates to the centerline of the channel as its equilibrium location. The LBM predicts this migration. There are some quantitative differences. For example, when the initial location is about y/H of 0.2, the particle reaches the axis at x/H of 7 in the LBM whereas the results of Feng *et al.* [6] show the equilibrium being reached at about 9.

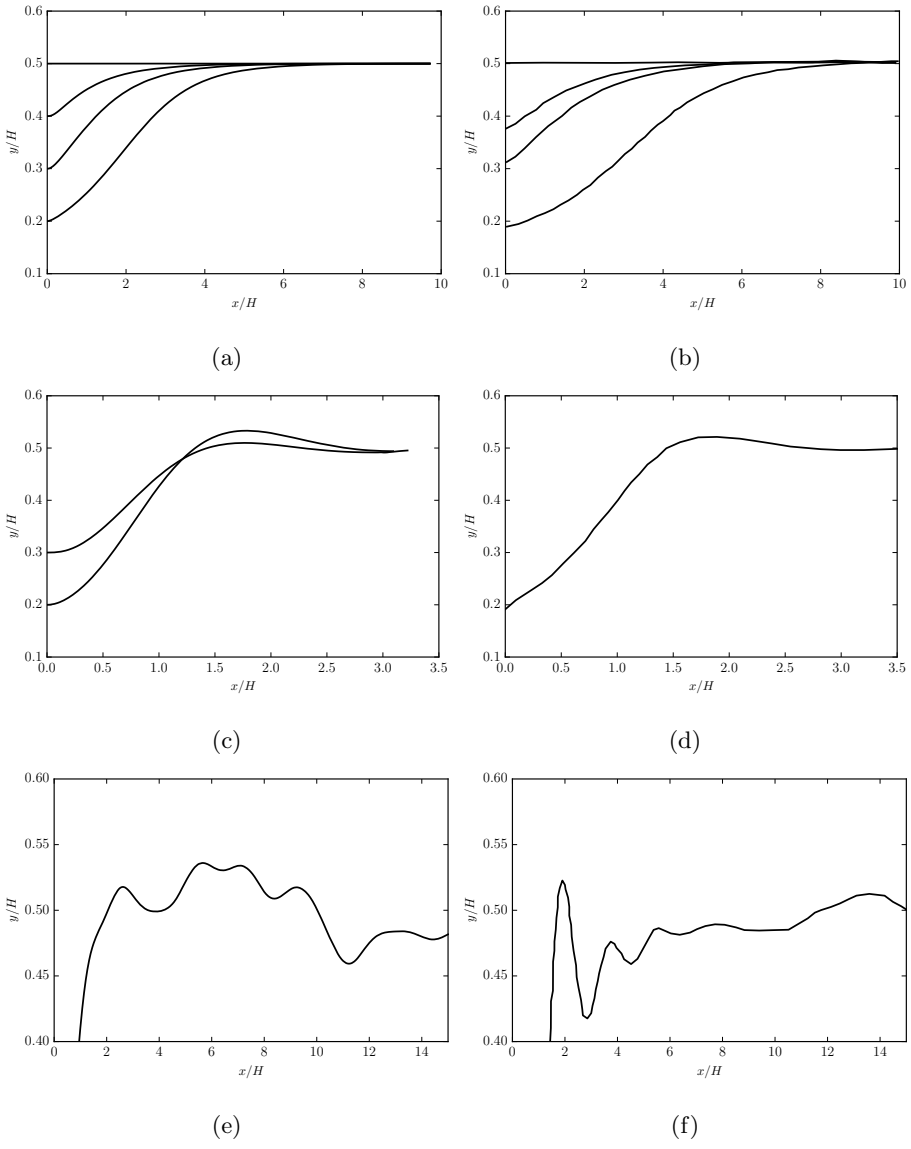

Figure 7: Particle migration trajectories at a) Regime A LBM (Re = 1.224); b) Regime A Feng *et al.* [6] (Re = 0.522) c) Regime B LBM (Re = 10.8); d) Regime B Feng *et al.* [6] (Re = 3.23) e) Regime C LBM (Re = 48.15); f) Regime C *et al.* [6] (Re = 27.6)

Table 1: Particle migration regimes for a particle settling in a channel under gravity [6].

Regime	Description	Approx. Re number range
A	Steady equilibrium with monotonic approach	0.1∼2
B	Steady equilibrium with transient overshoot	3∼20
C	Weak oscillatory motion	20∼60
D	Strong oscillatory motion	60∼300
E	Irregular oscillatory motion	>300

The difference is likely on account of the difference in Re number between our simulations and that of Feng *et al.* [6]. We have computed one case where the Re number is reasonably close to that of Feng *et al.* [6]. Figure 8 shows a quantitative comparison for this particular case. It can be seen that there is good agreement between the current work and that of Feng *et al.* [6]. Regimes D and E are difficult to simulate using the LBM as implemented in this work. To achieve the high Re numbers required to simulated these regimes, the relaxation parameter (τ) in the BGK collision operator (Eq. 8) has to be close to 0.5 which would make the computations unstable. The multiple relaxation time (MRT) implementation [34, 35] of the LBM can, however, be employed to address this challenge. All computations reported below are for a particle Re number less than 20. The Re number based on the channel height would be 4-6 times higher than the Re number based on the particle diameter.

3.2. Neutrally Buoyant Particle In A Channel Flow

The next set of simulations considered the motion of a neutrally buoyant particle in a channel flow. A Reynolds number Re_p based on the particle radius r and height of the channel H is defined as follows

$$Re_p = \frac{U_{max} r^2}{\nu H} \tag{10}$$

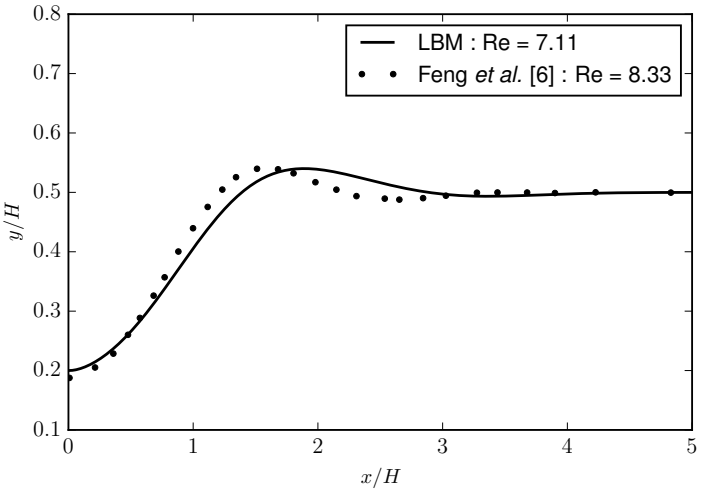

Figure 8: Quantitative comparison of particle migration trajectories at Regime B

where U_{max} is the maximum velocity of the fluid, and ν is the viscosity of the fluid.

For this set of simulations, Feng *et al.* [7] observed the Segré-Silberberg effect where the particle migrates to a position between the centerline and the wall irrespective of the position from which it is released. Figure 9 shows a comparison between the particle trajectory obtained in this work and that of Feng *et al.* [7] at a Re_p of 0.875. For this Re_p, Feng *et al.* [7] have reported only the trajectory for the particle released from the centerline. There is a good agreement between the result of Feng *et al.* [7] and our results. From the LBM computations, it can be seen that when the particle is released from the center, it takes a longer time to come to its equilibrium position than when it is released at other locations. The equilibrium position also seems to be at some distance midway between the wall and the centerline. These trends are in agreement with the results of Feng *et al.* [7] for a Re_p of 0.625 (not shown here). The mechanism of this particle migration is explained by Feng *et al.* [7] and a brief description will now be provided.

The Saffman lift force is a lateral force that tends to move a particle that

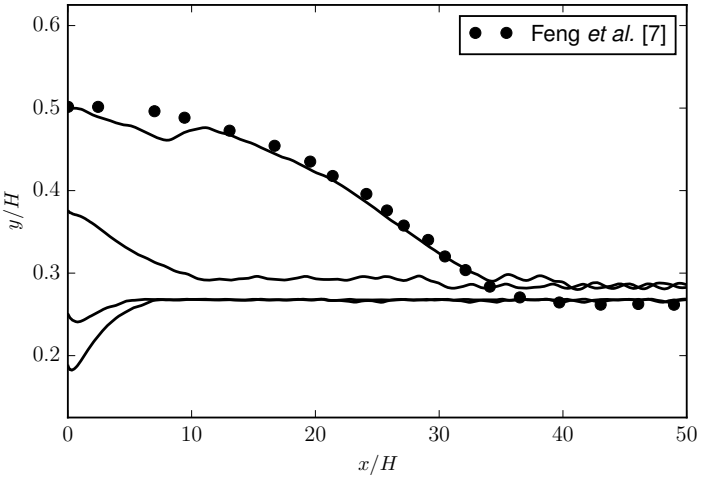

Figure 9: Comparison of the particle migration trajectories for a neutrally buoyant particle in a channel flow at $Re_p = 0.875$.

either leads or lags the fluid velocity. In a linear velocity profile, the Saffman lift would push a particle that leads the fluid toward the region with low velocity and vice versa. Figure 10a shows a particle in a uniform shear flow. If the particle lags the fluid velocity, then the relative velocity (see Fig. 10b) on top of the particle would be higher than that on its bottom. This develops a high pressure beneath the particle pushing it upwards. Similarly, if the particle leads the fluid velocity, then the relative velocity (see Fig. 10c) will be higher beneath the particle which develops a high pressure on top of the particle pushing it downward.

However, in the case of a particle in a channel flow, the curvature in the velocity profile of the undisturbed flow tends to reverse this trend. Figure 11 shows the relative velocity of the fluid with respect to the particle for two possible cases: one with a large slip velocity where the particle lags the fluid in all regions and another with a small slip velocity where the particle velocity lags the fluid. It should be noted that since the particle is released with zero velocity, the particle would lag behind the fluid most of the time. However, it is possible that when a particle is pushed from a streamline with a higher velocity

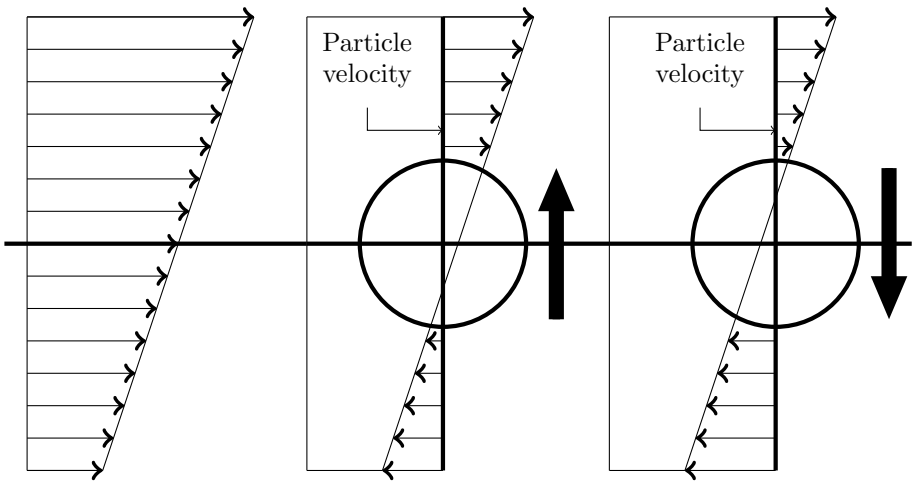

Figure 10: Schematic of a particle in a uniform shear flow; (a) linear velocity profile, (b) relative velocity of fluid when particle is lagging fluid, (c) relative velocity of fluid when particle is leading fluid.

to one with lower velocity, it may lead the fluid for a short time. When the slip velocity is large, the relative velocity of fluid on the free stream side of the particle would be higher than that on its wall side. This would cause a high pressure buildup beneath the particle pushing it away from the wall. When the slip velocity is small, the behavior is different. Consider the sketch in Fig. 11b. We can see that the magnitude of relative velocity is higher on its wall side than on its free stream side. This causes a high pressure buildup on top of the particle which pushes it toward the wall. Hence, in this case, for most part of the particle motion (except the initial transient time interval), the Saffman lift pushes the particle toward the wall. The direction of Saffman lift is the same even if the particle leads the fluid with a small slip velocity. The center will be an equilibrium position where there would be no effect of Saffman lift on the particle.

Figure 12a shows the velocity contour of the fluid during one of the simulations in which the particle is moving. The particle position at the time when the

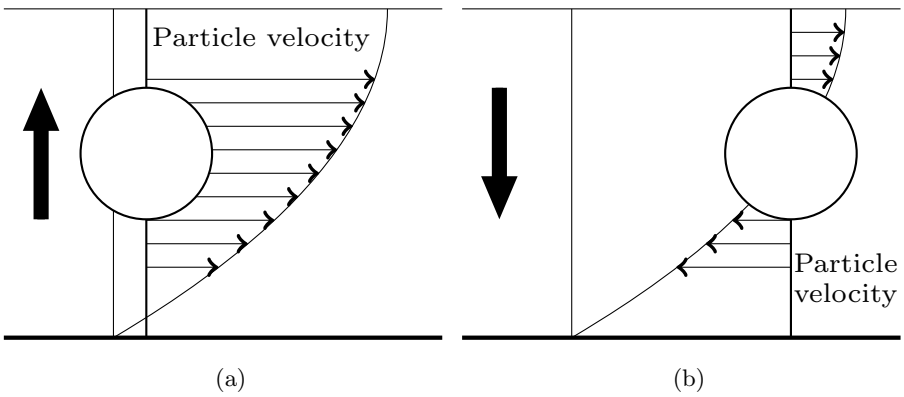

Figure 11: Schematic illustration of the relative velocity of a particle in a parabolic velocity profile; a) large slip velocity b) small slip velocity.

velocity contour plot is taken is also shown. The undisturbed velocity profile is a parabolic profile. It can be seen that the presence of the particle alters the velocity distribution in its vicinity. Figure 12b shows the relative velocity magnitude of the flow with respect to the particle. It is evident from this figure that the velocity between the particle and the bottom wall is higher than the velocity on the other side. This causes a high pressure buildup on top of the particle which pushes it toward the wall.

The movement of the particle toward the wall is opposed by wall repulsion [6, 7]. This is a force that arises when there is a relative motion between the wall and the particle. During this relative motion, a thin layer of fluid is squeezed in the gap between the particle and the wall, increasing the pressure which pushes the particle away from the wall. This force is similar in nature to lubrication force. If only wall repulsion force existed, the equilibrium position would be where wall repulsion from the top and bottom wall are equal and opposite each other. This would correspond to the centerline of the channel.

The Magnus lift force arises on account of the rotation of the particle. When a particle rotates in a uniform flow, it would push fluid in the direction of motion on one side and against the direction of motion in the opposite side. This would cause a velocity gradient, which in turn causes a pressure gradient pushing the

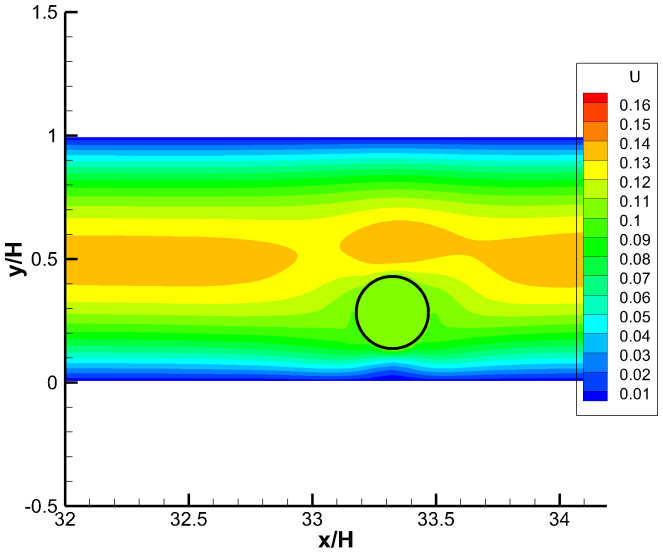

(a)

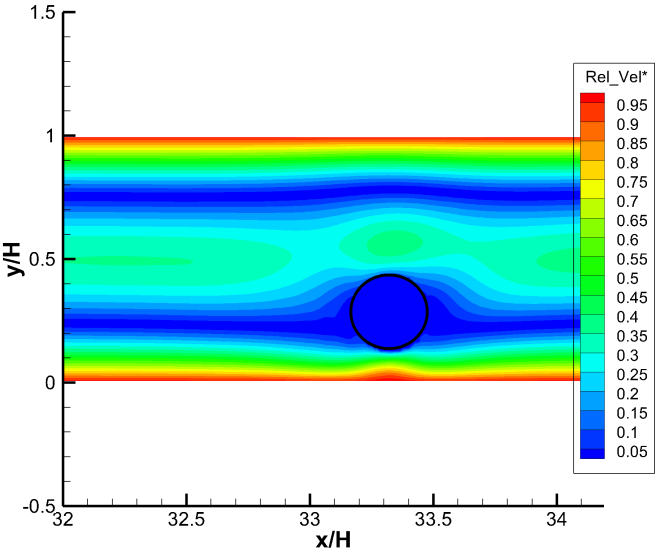

(b)

Figure 12: (a) Velocity contour (b) Relative velocity magnitude of the fluid with respect to the particle

particle toward the low pressure region. At the centerline of the channel, the particle would not rotate since the undisturbed velocity profile is symmetric about the center line and hence the center would be an equilibrium position. Thus, if a particle is released from the centerline, it would not experience the Magnus lift force. Now, if the particle is displaced slightly from the center, Saffman lift pushes the particle toward the wall and it keeps moving until Saffman lift, Magnus lift and wall repulsion are in balance. This would be a stable equilibrium for the particle and it would be at a location between the wall and the centerline. The centerline is not a stable equilibrium. It will be shown later in this work that the Magnus lift force also acts in the same direction as the Saffman lift.

These studies show that the LBM can be employed to study particle migration trajectories and elucidate the physics. In the next section, we will employ the method to investigate the effect of Stokes (St) number on the migration trajectories and determine the controlling mechanisms

4. Results and Discussion

Our work is two-dimensional in nature employing the same code that we used for the studies above. Table 2 shows a list of cases that are examined in this work. The particle time constant for cases 1-4 are calculated using equation 1 while that for the other cases are calculated using equation 2.

Figure 13 shows the trajectory of the particle in the channel for four different St numbers (0.5, 1.6, 11.4 and 14.2). The St number is varied by changing the density of the particle. The particle is released from a location $y/H = 0.25$. The channel height is 4 times the particle diameter. It can be seen that for St = 0.5, the particle behaves as a neutrally buoyant particle in a channel flow exhibiting the Segré-Silberberg effect (See Fig. 8 and related discussion). When St = 1.6, the particle behavior is not very different from St = 0.5, but minor oscillations about the equilibrium position is evident. When St = 11.4, the particle moves all the way to the center of the channel and farther towards the top wall and settles in its equilibrium position close to the top wall. The initial motion of

Table 2: A list of cases examined in this study

Case	ρ_p	ρ_f	U_{max}	St number
1	0.72	1.0	0.16	0.5
2	3.36	1.0	0.16	1.6
3	26.88	1.0	0.16	11.4
4	33.60	1.0	0.16	14.2
5	96.00	1.0	0.16	40
6	120.00	1.0	0.16	50
7	168.00	1.0	0.16	70
8	240.00	1.0	0.16	100

the particle toward the top wall is just a transient effect. It should be noted that the channel flow has two equilibrium positions, one near the top wall and one near the bottom wall on account of its symmetry about the center line. For clarity, 1-y/H is plotted against x/H for this case. It is seen that the particle oscillation about the equilibrium position has now become noticeable. Similar behavior is observed for St = 14.2, but the mean is more close to the centerline.

For the lower St number cases, the behavior of particles settling at a location between the wall and the axis is similar to that of a neutrally buoyant particle and has been explained by Feng *et al.* [7] in terms of Saffman lift, Magnus lift, curvature of the undisturbed velocity profile and wall repulsion.

It is of interest to understand why the particle with the larger St number oscillates about this equilibrium position rather than remain at the position. A particle with a larger St number has a longer response time which implies that it has a higher inertia than a particle with a lower St number. The particle is released from $y/H = 0.25$. During the initial transient time, Saffman lift pushes the particle away from the wall owing to the large slip velocity. Hence the particle moves toward the center. As it comes closer to the center, the particle's

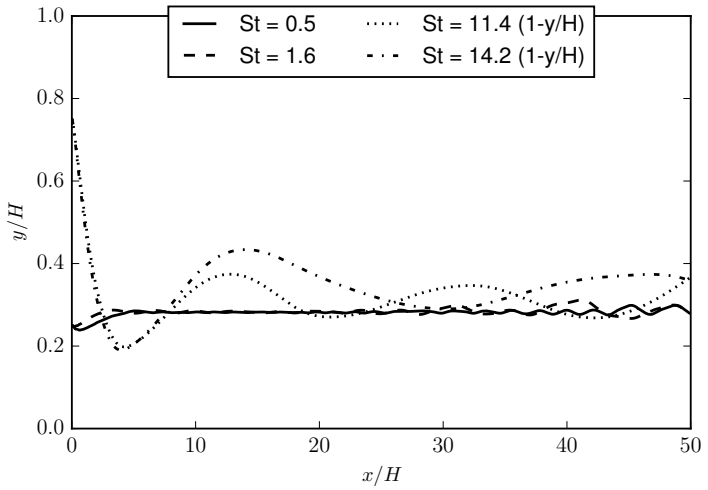

Figure 13: Particle migration trajectories for different St numbers. (For $St = 11.4$ and $St = 14.2$, 1-y/H is plotted against x/H)

velocity in the axial direction increases and so its slip velocity decreases. As a result of inertia, the particle moves beyond the center line and moves closer to the equilibrium position near the top wall. Since the slip velocity is now small, Saffman lift acts to push the particle toward the wall and the particle moves upwards. As it approaches the equilibrium position, the sum of the Saffman lift, Magnus lift and wall repulsion force decreases. But, due to its inertia, it continues to move further toward the wall until the wall repulsion overcomes the inertial effects. At this position, the wall repulsion is higher than the Saffman and Magnus lift and this unbalanced force causes the particle to move back toward its equilibrium position. Again, due to inertia it will overshoot a short distance and then move back toward the wall and this oscillation continues. Mortazavi and Tryggvason [8] have reported similar oscillations of drops in a channel flow at high Re number. Further studies should be conducted to see if the oscillations are just transient effects.

In order to determine how the particle behaves when the St number is increased further, four more cases are considered with St number of 40, 50, 70 and 100. The trajectories for these particles are shown in Fig. 14. Increasing

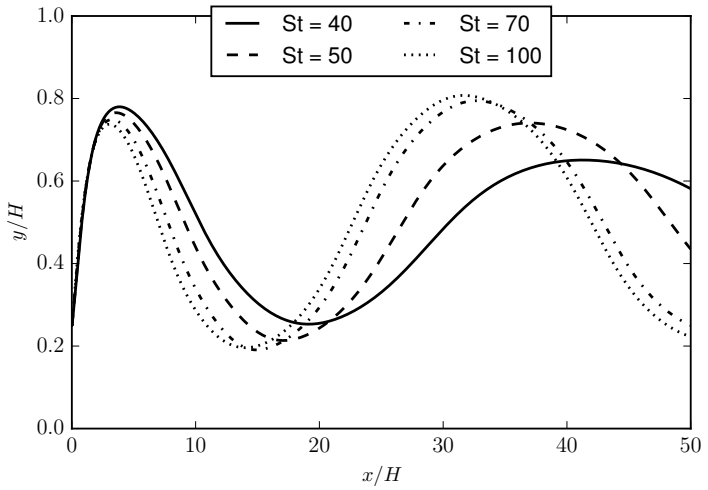

Figure 14: Particle migration trajectories for high St numbers

the St number appears to increase the amplitude although changes are small for the range considered. Compared to the result for St number of 11.4 shown in Fig. 13, the frequency of the oscillation for St number of 50 in Fig. 14 is about a factor of four lower. The larger amplitude and the lower frequency are consistent with larger inertia particles adjusting slower to changes in the forces.

Simulations are carried out to determine if the initial position at which the particle is released from has an effect on its equilibrium position. Figure 15 shows the migration trajectories for particles released from varying y/H distance. It can be seen that the particle migrates to the same position irrespective of the location from which it is released. Also, it should be noted that when the particle is released from the center it travels a longer distance before reaching its equilibrium position. This is because, as mentioned earlier, the centerline is also an equilibrium position but not a stable one. However, depending on the initial location there seems to be a minor difference in the amplitude of the oscillations. Particles released closer to the equilibrium position have smaller amplitude of oscillations than those released farther away.

Next, the effect of particle size relative to the channel width, i.e. H/d, for a

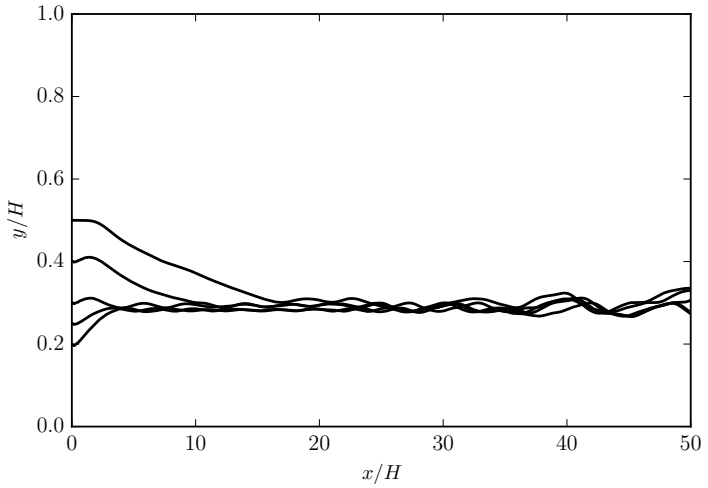

Figure 15: Effect of initial position on the particle migration trajectories ($St = 1.6$)

given St number is studied. Figure 16 shows the particle migration trajectories for 3 different H/d ratios. The velocity of the fluid and density of the particle are changed so that the St number remains the same in all cases. As the H/d ratio becomes larger, the particle moves closer to the wall. This is because as the relative size of the particle decreases, the wall repulsion force decreases, allowing the Saffman and Magnus lift to push the particle closer to the wall. It is also seen that at higher H/d ratios, the particle begins to exhibit oscillations. This can be explained by understanding the role of the Magnus lift in more detail. Feng *et al.* [7] report that the presence of a wall near the particle tends to suppress the rotation of the particle and thereby reduce the Magnus lift force acting on the particle. Figure 17 shows the particle migration trajectories for the low St number cases with and without the Magnus force. It is evident from this figure that the equilibrium position of the particle shifts toward the centerline, from y/H value of about 0.28 to about 0.4. Furthermore, the oscillations that are seen for the St = 11.4 and St = 14.2 cases are not seen when Magnus lift force is absent. Figure 18 shows similar results for the high St number cases. For this range of St numbers, it can be seen that the oscillation persists but its amplitude

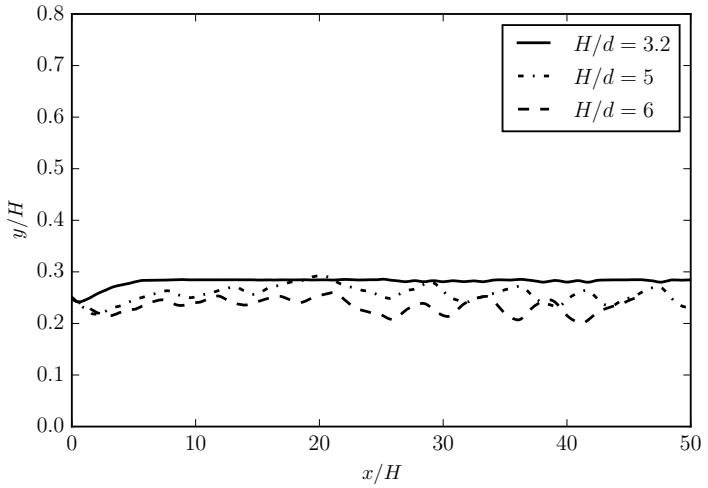

Figure 16: Particle migration trajectories for different H/d ratios ($St = 0.5$)

is reduced because the wall repulsion has to overcome only the Saffman lift and hence the particle is pushed away from the wall to a greater distance than in the case with the Magnus lift force The implication is that the Magnus force adds to the Saffman force to move the particle toward the wall. The absence of the Magnus force does not remove the oscillations. It just changes the St for which the oscillation sets in. Increasing the H/d ratio increases the effective distance between the wall and the particle. Hence the Magnus lift force acting on the particle increases and the St number at which the oscillations appear decreases.

5. Conclusion

The lattice-Boltzmann method (LBM) is employed to carry out simulations of particle motion in a channel for various Stokes (St) numbers. It is shown that the St number influences the motion. Particles with low St number behave similar to a neutrally buoyant particle in a channel flow exhibiting the Segr-Silberberg effect. They move to an equilibrium position that is between the wall and the axis. This lateral migration of the particle arises as a result of three different forces acting on the particle namely: the Saffman lift, the Magnus

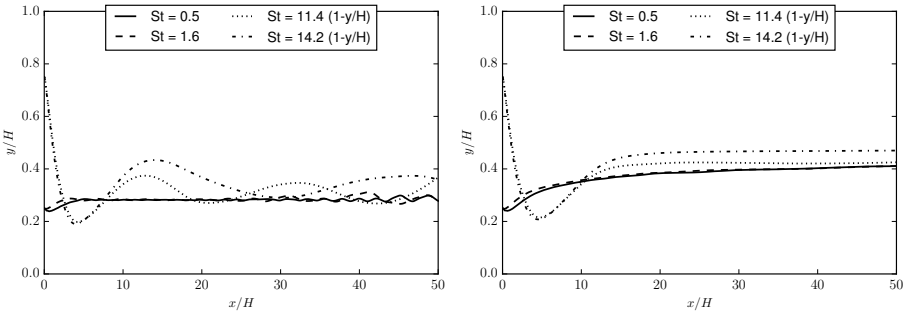

(a) (b)

Figure 17: Particle migration trajectories for particles a) with rotation and b) without rotation, i.e. no Magnus force

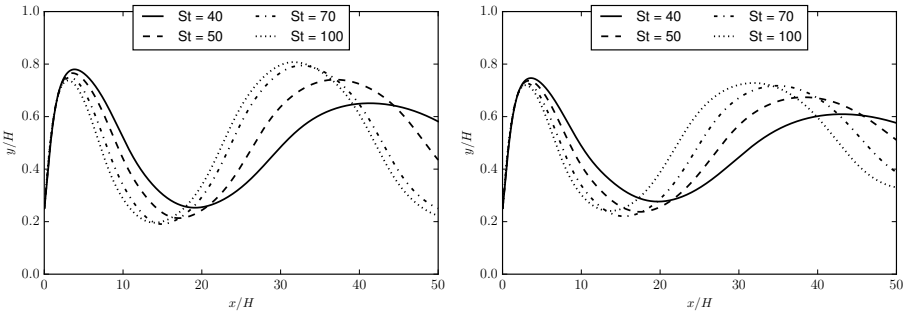

(a) (b)

Figure 18: Particle migration trajectories for higher St number cases a) with rotation b) without rotation

lift and wall repulsion. Except for an initial transient time, the Saffman and Magnus lift forces act in the same direction and push the particle toward the wall while the wall repulsion acts to push the particle away from the wall. The particle settles at an equilibrium location where these three forces balance. As the St number is increased, the particle exhibits an oscillatory behavior about its equilibrium position. The oscillation amplitude and time period increases with increasing St number. The oscillations arise from the increasing importance of inertial effects. Increasing the ratio of the channel width to the particle diameter for a given St number reduces the effect of wall repulsion due to which the particle moves closer to the wall. Increasing the H/d ratio decreases the St number at which the oscillations begin to occur.

Acknowledgments

We thank Professor Graham Nathan and Dr. Timothy Lau, University of Adelaide, Australia, for the useful discussions we had with them regarding particle migration.

References

[1] Segré G., Silberberg A., Behaviour of macroscopic rigid spheres in Poiseuille flow Part 1. Determination of local concentration by statistical analysis of particle passages through crossed light beams, Journal of Fluid Mechanics (1962) 115–135.

[2] Segré G., A. Silberberg, Behaviour of macroscopic rigid spheres in Poiseuille flow Part 2. Experimental results and interpretation, Journal of Fluid Mechanics (1962) 136–157.

[3] F. P. Bretherton, The motion of rigid particles in a shear flow at low Reynolds number, Journal of Fluid Mechanics (1962) 284–304.

[4] P. G. Saffman, The lift on a small sphere in a slow shear flow, Journal of Fluid Mechanics 22 (1965) 385–400. doi:10.1017/S0022112065000824.

URL http://www.journals.cambridge.org/abstract_S0022112065000824

[5] J. B. McLaughlin, The lift on a small sphere in wall-bounded linear shear flows, Journal of Fluid Mechanics 246 (1993) 249–265. doi:10.1017/S0022112093000114.
URL http://www.journals.cambridge.org/abstract_S0022112093000114

[6] J. Feng, H. H. Hu, D. D. Joseph, Direct simulation of initial value problems for the motion of solid bodies in a Newtonian fluid Part 1. Sedimentation, Journal of Fluid Mechanics 261 (1994) 95–134.

[7] J. Feng, H. H. Hu, D. D. Joseph, Direct simulation of initial value problems for the motion of solid bodies in a Newtonian fluid. Part 2. Couette and Poiseuille flows, Journal of Fluid Mechanics 277 (1994) 271–301. doi:10.1017/S0022112094002764.
URL http://www.journals.cambridge.org/abstract_S0022112094002764

[8] S. Mortazavi, G. Tryggvason, A numerical study of the motion of drops in Poiseuille flow. Part 1. Lateral migration of one drop, Journal of Fluid Mechanics 411 (2000) 325–350.

[9] L. Zeng, S. Balachandar, P. Fischer, Wall-induced forces on a rigid sphere at finite Reynolds number, Journal of Fluid Mechanics 536 (2005) 1–25. doi:10.1017/S0022112005004738.
URL http://www.journals.cambridge.org/abstract_S0022112005004738

[10] A. Nourbakhsh, S. Mortazavi, Y. Afshar, Three-dimensional numerical simulation of drops suspended in Poiseuille flow at non-zero Reynolds numbers, Physics of Fluids 23 (12) (2011) 123303. doi:10.1063/1.3663565.
URL http://scitation.aip.org/content/aip/journal/pof2/23/12/10.1063/1.3663565

[11] T. C. Lau, G. J. Nathan, Influence of Stokes number on the velocity and concentration distributions in particle-laden jets, Journal of Fluid Mechanics 757 (2014) 432–457. doi:10.1017/jfm.2014.496.
URL http://www.journals.cambridge.org/abstract_S0022112014004960

[12] J. K. Eaton, J. R. Fessler, Preferential Concentration of Particles by Turbulence, International Journal of Multiphase Flow 20 (94) (1994) 169–209. doi:0301-9322(94).

[13] A. J. C. Ladd, Numerical simulations of particulate suspensions via a discretized Boltzmann equation. Part 1. Theoretical foundation, Journal of Fluid Mechanics 271 (1994) 285–309.

[14] A. J. C. Ladd, Numerical simulations of particulate suspensions via a discretized Boltzmann equation. Part 2. Numerical results, Journal of Fluid Mechanics 271 (1994) 311–339.

[15] C. K. Aidun, Y. Lu, E.-J. Ding, Direct analysis of particulate suspensions with inertia using the discrete Boltzmann equation, Journal of Fluid Mechanics 373 (1998) 287–311.

[16] D. Qi, Lattice-Boltzmann simulations of particles in non-zero-Reynolds-number flows, Journal of Fluid Mechanics 385 (1999) 41–62.

[17] D. Qi, Lattice-Boltzmann simulations of fluidization of rectangular particles, International Journal of Multiphase Flow 26 (2000) 421–433.

[18] D. Qi, Simulations of fluidization of cylindrical multiparticles in a three-dimensional space, International Journal of Multiphase Flow 27 (2001) 107–118.

[19] D. Qi, L. Luo, R. Aravamuthan, W. Strieder, Lateral Migration and Orientation of Elliptical Particles in Poiseuille Flows, Journal of Statistical Physics 107 (April) (2002) 101–120.

[20] Z.-G. Feng, E. E. Michaelides, The immersed boundary-lattice Boltzmann method for solving fluidparticles interaction problems, Journal of Computational Physics 195 (2) (2004) 602–628. doi:10.1016/j.jcp.2003.10.013.
URL http://linkinghub.elsevier.com/retrieve/pii/S0021999103005758

[21] Z.-G. Feng, E. E. Michaelides, Proteus: a direct forcing method in the simulations of particulate flows, Journal of Computational Physics 202 (1) (2005) 20–51. doi:10.1016/j.jcp.2004.06.020.
URL http://linkinghub.elsevier.com/retrieve/pii/S0021999104002669

[22] Z.-G. Feng, E. E. Michaelides, Robust treatment of no-slip boundary condition and velocity updating for the lattice-Boltzmann simulation of particulate flows, Computers & Fluids 38 (2) (2009) 370–381. doi:10.1016/j.compfluid.2008.04.013.
URL http://linkinghub.elsevier.com/retrieve/pii/S0045793008001060

[23] M. Bouzidi, M. Firdaouss, P. Lallemand, Momentum transfer of a Boltzmann-lattice fluid with boundaries, Physics of Fluids 13 (11) (2001) 3452. doi:10.1063/1.1399290.
URL http://scitation.aip.org/content/aip/journal/pof2/13/11/10.1063/1.1399290

[24] A. Joshi, Y. Sun, Multiphase lattice Boltzmann method for particle suspensions, Physical Review E 79 (6) (2009) 066703. doi:10.1103/PhysRevE.79.066703.
URL http://link.aps.org/doi/10.1103/PhysRevE.79.066703

[25] X. Shi, N. Phan-Thien, Distributed Lagrange multiplier/fictitious domain method in the framework of lattice Boltzmann method for fluidstructure interactions, Journal of Computational Physics 206 (1) (2005) 81–94. doi:10.1016/j.jcp.2004.12.017.

URL http://linkinghub.elsevier.com/retrieve/pii/S0021999104004942

[26] Z.-G. Feng, E. E. Michaelides, Interparticle forces and lift on a particle attached to a solid boundary in suspension flow, Physics of Fluids 14 (1) (2002) 49. doi:10.1063/1.1426389.
URL http://scitation.aip.org/content/aip/journal/pof2/14/1/10.1063/1.1426389

[27] N.-Q. Nguyen, A. J. C. Ladd, Lubrication corrections for lattice-Boltzmann simulations of particle suspensions, Physical Review E 66 (4) (2002) 046708. doi:10.1103/PhysRevE.66.046708.
URL http://link.aps.org/doi/10.1103/PhysRevE.66.046708

[28] C. K. Aidun, J. R. Clausen, Lattice-Boltzmann Method for Complex Flows, Annual Review of Fluid Mechanics 42 (1) (2010) 439–472. doi:10.1146/annurev-fluid-121108-145519.
URL http://www.annualreviews.org/doi/abs/10.1146/annurev-fluid-121108-145519

[29] R. Mei, D. Yu, W. Shyy, L.-S. Luo, Force evaluation in the lattice Boltzmann method involving curved geometry, Physical Review E 65 (4) (2002) 041203. doi:10.1103/PhysRevE.65.041203.
URL http://link.aps.org/doi/10.1103/PhysRevE.65.041203

[30] S. Chen, D. Martínez, R. Mei, On boundary conditions in lattice Boltzmann methods, Physics of Fluids 8 (9) (1996) 2527–2536. doi:10.1063/1.869035.
URL http://scitation.aip.org/content/aip/journal/pof2/8/9/10.1063/1.869035

[31] S. Succi, The Lattice Boltzmann Equation for Fluid Dynamics and Beyond, Oxford Science Publications, 2001.

[32] S. Chen, Z. Wang, X. Shan, G. D. Doolen, Lattice Boltzmann computational fluid dynamics in three dimensions, Journal of Statistical Physics 68 (1992) 379–400. doi:10.1007/BF01341754.
URL http://link.springer.com/10.1007/BF01341754

[33] X. He, Q. Zou, L.-s. Luo, M. Dembo, Analytic Solutions of Simple Flows and Analysis of Nonslip Boundary Conditions for the Lattice Boltzmann BGK Model, Journal of Fluid Mechanics 87 (1997) 115–136.

[34] K. N. Premnath, J. Abraham, Three-dimensional multi-relaxation time (MRT) lattice-Boltzmann models for multiphase flow, Journal of Computational Physics 224 (2007) 539–559. doi:10.1016/j.jcp.2006.10.023.
URL http://linkinghub.elsevier.com/retrieve/pii/S0021999106004815

[35] M. McCracken, J. Abraham, Multiple-relaxation-time lattice-Boltzmann model for multiphase flow, Physical Review E 71 (3) (2005) 036701. doi:10.1103/PhysRevE.71.036701.
URL http://link.aps.org/doi/10.1103/PhysRevE.71.036701